Facies (2007) 53:189–208
DOI 10.1007/s10347-006-0098-5

ORIGINAL ARTICLE

Aragonite and calcite cementation in "boulder-controlled" meteoric environments on the Fern Pass rockslide (Austria): implications for radiometric age dating of catastrophic mass movements

Marc Ostermann · Diethard Sanders · Christoph Prager · Jan Kramers

Received: 12 April 2006 / Accepted: 29 November 2006 / Published online: 9 February 2007

Abstract On the Fern Pass rockslide (Eastern Alps, Austria), projecting boulders collected surface runoff and delayed percolation of water into the rockslide mass, leading to decimetre-scale, fluctuating, phreatic/vadose diagenetic systems along their contact. In these systems, aragonite and calcite precipitation were nourished mainly by dissolution of carbonate-rock flour. Cement precipitation was limited to southern- and eastern-exposed "runoff haloes" of boulders and mainly resulted in cemented breccias. Aragonite precipitation was related to dissolved Mg^{2+} and/or to high $CaCO_3$ supersaturation in evaporative-concentrated pore waters. Early aragonite cement yielded a $^{234}U/^{230}Th$ age of 4,150 ± 100 years. Relative to other radiometric ages (^{36}Cl, ^{14}C; by other authors) for the rockslide event, the U–Th age of the aragonite is the most precise proxy of depositional age. Carbonate cements are present in other rockslide and rockfall deposits also. U–Th dating of such cements is thus a comparatively rapid and inexpensive method of minimum-age dating catastrophic mass movements.

M. Ostermann · D. Sanders (✉)
Institute of Geology and Palaeontology,
University of Innsbruck, Innrain 52, 6020 Innsbruck, Austria
e-mail: Diethard.G.Sanders@uibk.ac.at

C. Prager
alpS - Centre for Natural Hazard Management,
Grabenweg 3, 6020 Innsbruck, Austria

J. Kramers
Institute of Geological Sciences,
University of Bern, CH-3012 Bern, Switzerland

Keywords Eastern Alps · Rockslide · Sturzstrom · Vadose diagenesis · Aragonite · Thorium–uranium · Holocene

Introduction

In mountain areas subject to uplift and fluvioglacial erosion, catastrophic rockslides or sturzstroms are among the most significant processes of large-scale, long-term erosion and orogenic mass balance (Summerfield 1991; Gilchrist et al. 1994). Sturzstroms originate when a large mass of rock slides or falls at once down slope, leading to a highly mobile, fast-moving avalanche of extremely poorly sorted clastic material (Erismann and Abele 2001). In the Alps, rockslides are the most destructive geological events to humans and facilities (Abele 1974). Aside of well-documented sturzstroms in historic times, however, age dating of older rockslide deposits has been notoriously difficult due to scarcity of chronostratigraphic markers. Rockslides and rockfalls have been dated by ^{14}C age dating of organic remnants that are preserved in successions of rockslide-dammed lakes or that became entrapped or overridden by the rocky debris (Heuberger 1966; Patzelt and Poscher 1993; Jerz and Poschinger 1995; Antognini and Volpers 2002). In recent years, direct age determination of rockslides became possible by exposure dating of boulder surfaces and scarps with cosmogenic nuclides (Ivy-Ochs et al. 1998; Gosse and Philips 2001). Alternatively, as reported herein, sturzstroms may also be minimum-age dated by diagenetic products such as carbonate cements formed in meteoric environments. Previously, lithified portions of rockslide intervals were not systematically searched

for, yet they are probably common, at least in rockslides with a high proportion of carbonate rock fragments. Intense abrasion during the rockslide event, generating boulders embedded within abundant fine-grained matrix (Pollet and Schneider 2004), may favour meteoric lithification of sturzstrom deposits.

In the present paper, we describe the first minimum-age dating of an Alpine rockslide by the U–Th isochron method, applied to meteoric aragonite cement that precipitated shortly after the sturzstrom event. Aragonite commonly is considered a typical marine diagenetic product, but in the Alps, it is fairly common in terrestrial deposits, such as "cool-spring" tufas and coarse-grained hillslope deposits. For the Fern Pass rockslide, a comparison of these U–Th ages with radiocarbon ages and exposure ages produced by other workers (Prager et al. 2006a) indicates that the aragonite cementation age at present represents the most precise proxy of depositional sturzstrom age. We present a concept of cement precipitation in small-scale meteoric diagenetic systems that integrates the local setting of rockslide boulders and their size and exposition. Early formed carbonate cements are present in other coarse-grained Alpine-type subaerial deposits, also (see below). The cements of small-scale meteoric diagenetic systems thus provide an hitherto unexploited possibility for comparatively rapid and inexpensive minimum-age dating of mass failures.

Geological setting and characteristics of the rockslide

The Fern Pass rockslide is situated in the western part of the Northern Calcareous Alps (NCA) (Fig. 1). The NCA consist of stacked cover-thrust nappes, each dominated by Triassic shallow-water carbonates (Eisbacher and Brandner 1996; Schmid et al. 2004). With a volume of about 1 km^3, the rockslide of Fern Pass ranks the third largest of the Eastern Alps (Abele 1974). The sturzstrom originated from the southernmost portion of the Lechtal thrust nappe and left a deeply incised, east-facing scar (Fig. 1). In the studied area, the rock substrate consists mainly of the Hauptdolomit unit (Norian), a succession up to more than 2,000-m thick of stacked peritidal cycles that were subject to early post-depositional dolomitisation (Fruth and Scherreiks 1982). Within the Hauptdolomit, the Seefeld Formation is intercalated. The Seefeld Formation is a few hundred meters thick and consists of black shales and platy, organic-rich dolostones and limestones; these lithologies accumulated in a shallow intra-platform basin with anoxic bottom water (Brandner and Poleschinski 1986). The Seefeld Formation, in turn, is overlain by the Plattenkalk Formation (upper Norian *pro parte*; Donofrio et al. 2003) and, above, by bedded limestones and marls of the Kössen Formation (Rhaetian). The scarp area of the rockslide consists mainly of Seefeld Formation and, subordinately, of Plattenkalk and Kössen Formation, respectively.

Failure of the rockslide is related to the presence of three major fault and joint systems (cf. Eisbacher and Brandner 1996), including (1) east- to west-trending normal and reverse faults, (2) north-east-trending sinistral faults (Loisach-Fern Pass system), and (3) north-west-trending dextral faults (Nassereith–Marienberg transfer system) (Fig. 1). Intersection of these joint and fault systems results in disintegration of the carbonate succession into boulders to megaliths. After failure, the rockslide hit the opposite mountain slope, then branched (Fig. 1). The more voluminous northern branch came to rest, in its medial portions at least, on subglacial till. The distal part of the more confined, strongly deflected southern branch ran upon a substrate of water-saturated, glaciolacustrine deposits (sands, silts, clays) (Ampferer 1904, 1924; Prager and Zangerl 2005). Reflection seismics and ground-penetrating radar suggest that the rockslide deposit is about 500-m thick near Fern Pass but diminishes to some 10–30 m in the distal portion of the southern rockslide branch (Prager et al. 2006b). Whereas most previous investigators assigned a Late-Glacial to Holocene age to the rockslide, based on pollen analyses of lake deposits atop the rockslide (Fig. 1), Sarnthein (1940) concluded that the event happened about 2,000 BC. Subsequently, Abele (1964, 1974) differentiated between a late-glacial rockslide event and a post-glacial secondary event but later considered a Holocene age of the entire sturzstrom mass as being more likely (Abele 1997). Radiocarbon ages from rockslide-dammed torrent deposits (minimum age at least 3,080–3,380 cal. years BP; but the age of the base of the backwater succession is not yet established) and two ^{36}Cl exposure ages (3,400 ± 900 years, 4,800 ± 1,200 years) of slide planes of the rockslide scarp, with a mean age of 4,100 ± 1,300 years, indicate that the rockslide took place during the Middle Holocene (Prager et al. 2006a).

Today, the rockslide deposit is nearly completely covered by forest (mainly *Pinus*) and grass. The present surface of the rockslide is characterised by toma hills and transversal ridges as well as by elongate to subcircular depressions (some of them filled by lakes; Fig. 1). Fern Pass sturzstrom tomas are cone-shaped hills up to about 50- to 60-m high, with flank slopes typically between 35° and 40° (Fig. 2a). It has often been hypothesised that the tomas' cone shape resulted from glacial overprint (e.g. Wilhelmy 1972).

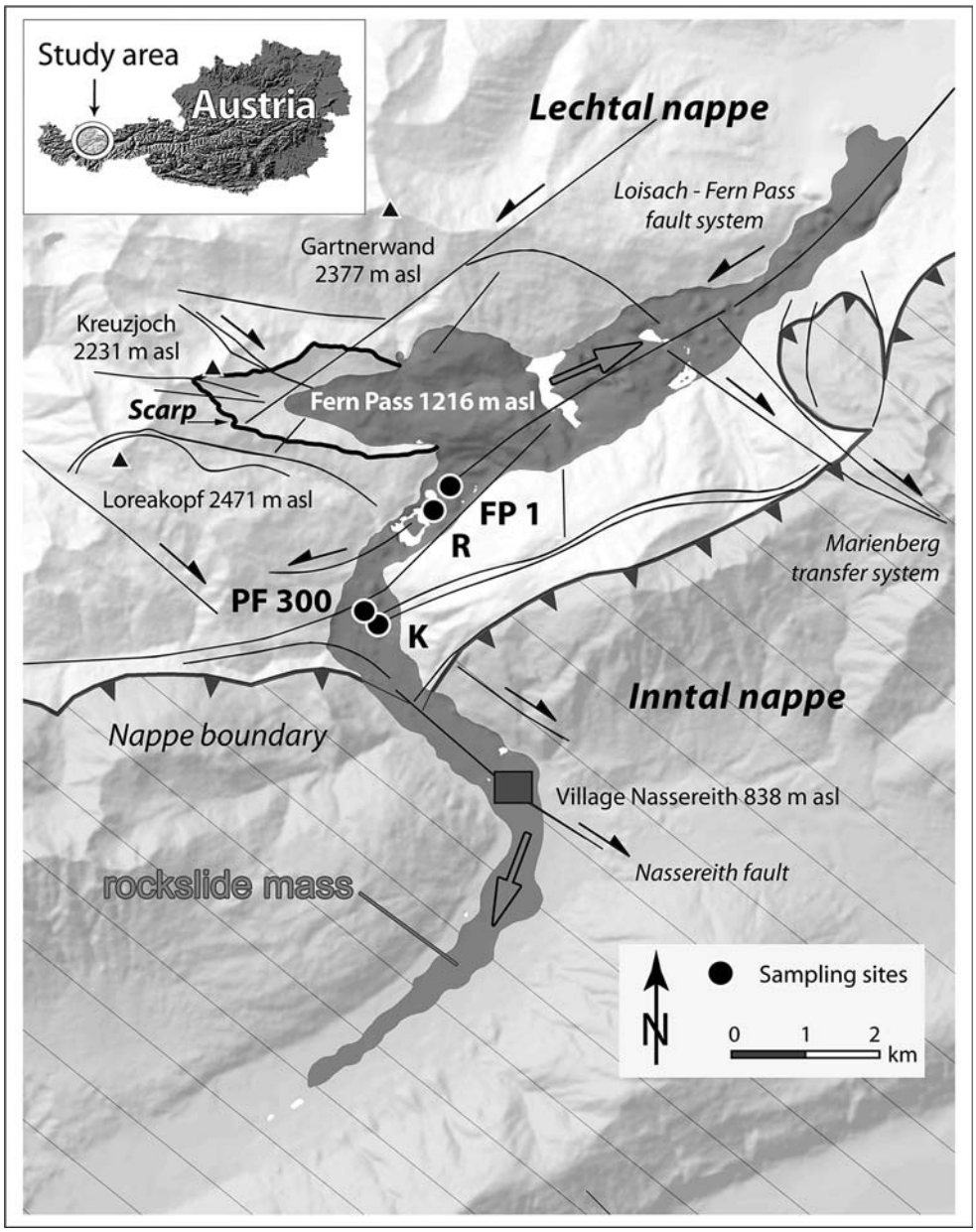

Fig. 1 Fern Pass rockslide (*shown in grey*) and its environs. *Inset* shows position in Austria. The study area consists of two stacked cover thrust nappes (Lechtal nappe, Inntal nappe) dominated by Triassic shallow-water carbonates. Aside of the nappe boundary, two main fault systems are present that controlled rockslide detachment. The detachment scarp (*heavy black line labelled by arrow*) of the sturzstrom delimits a deep, west–east elongate scar. *Black dots with letters* indicate sampling sites of breccias (*PF 300, R, K*) and of tufa limestone (*FP 1*) (see also Table 1). *White patches* are lakes atop the rockslide

At Fern Pass, however, no glacial overprint took place, yet these hills traditionally had been designated as tomas (Prager et al. 2006b). In the field, the exposed shallow-most portions of the rockslide are an extremely poorly sorted, unorganised deposit ranging in grain size from clay to boulders and, locally, to megaliths tens to hundreds of meters long. For the medial to distal portions of the rockslide, samples of the sediment fraction below the size of cobbles show that, today, the exposed parts of the deposit contain up to about 30% clay- to silt-sized carbonate-lithic matrix (Fig. 3). The matrix most probably was produced by dynamic disintegration, i.e. from attrition during movement of the rockslide. In the exposed portions of the sturzstrom deposit, the clasts typically are angular to subangular, whereas subrounded to well-rounded clasts are absent. Many gravel- to cobble-sized clasts are shattered and disintegrated along fractures with jig-saw-fitting boundaries (Fig. 2b). Prevalence of subangular clast shape in presence of fine-grained matrix was also observed in other rockslides, such as that of Flims, and results from continuous, intense clast fragmentation and abrasion during transport (cf. Pollet and Schneider 2004).

On the Fern Pass rockslide and in its environs, electrical conductivity (a parameter for concentration of dissolved ionic substances) of more than 180 springs was measured. Adjacent to the rockslide, springs emerging from the Hauptdolomit and Seefeld Formation show conductivities of typically 200–350 µS/cm.

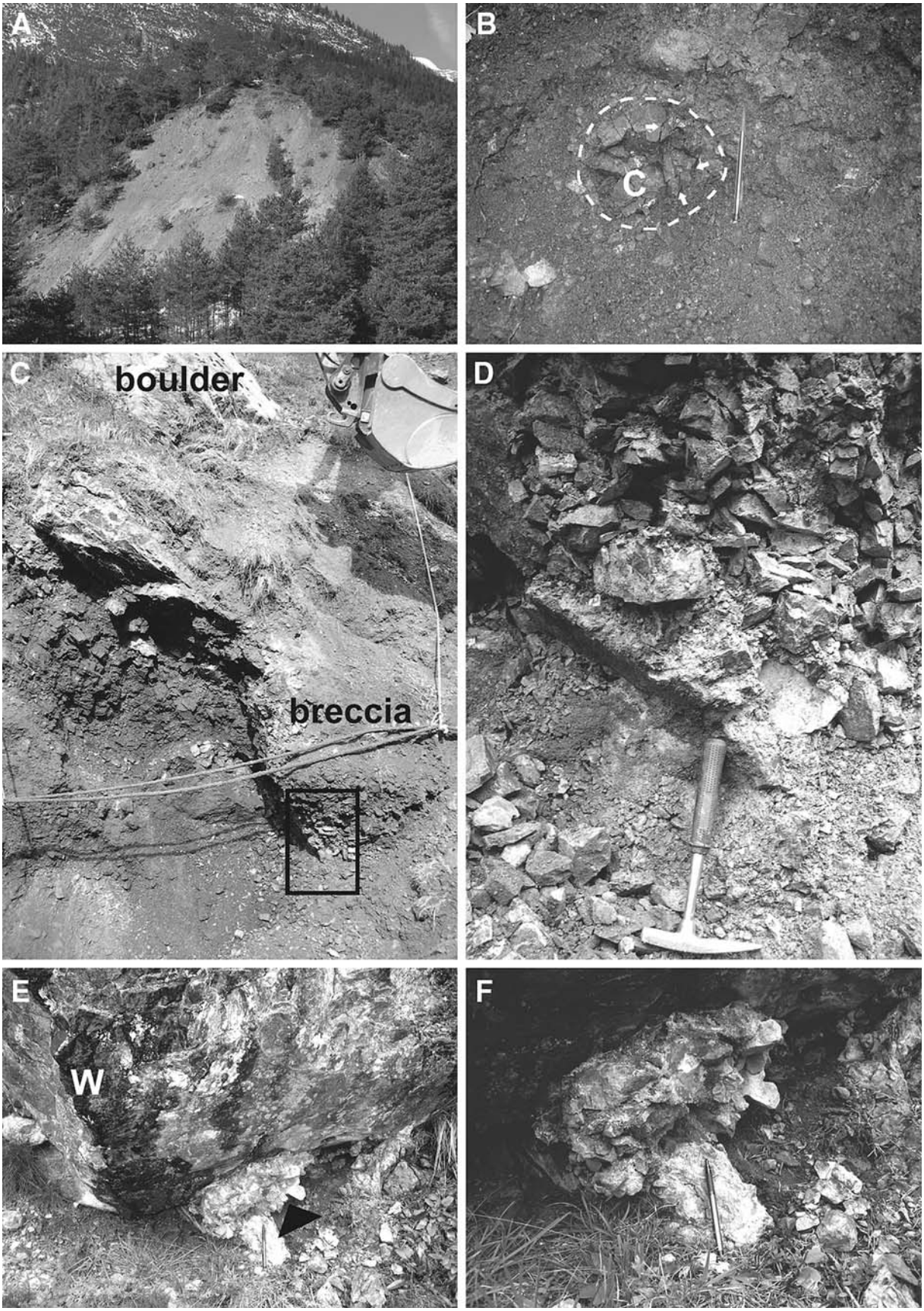
A
B
C
C
boulder
breccia
D
E
W
F

◀ **Fig. 2** Fern Pass rockslide and sampling locations of rockslide breccias. **a** Toma hill near Fern Pass. The toma consists of the same unsorted clastic material as the rest of the rockslide mass. Width of view about 60 m. **b** Man-made outcrop of unlithified rockslide deposit showing finer-grained matrix and a cobble (*c*, outlined by *dashed white line*) shattered along numerous open joints (some indicated by *white arrows*). *Pen* for scale is 14 cm. **c** Boulder projecting from the surface of the rockslide, underlain and onlapped by a cemented breccia of gravels to cobbles. Width of view about 2.5 m. The *black rectangle* marks the area shown in **d**. **d** Detail of breccia below boulder shown in the preceding photograph. Angular clasts of Hauptdolomit are lithified into a breccia by thin crusts of cement. *Hammer* for scale. **e** Location of breccia with Th–U age-dated aragonite cement. The breccia (indicated by *black arrowtip*) is cemented to the overhanging south-facing flank of a boulder of Hauptdolomit. The boulder is locally overrun by a film of water (*W*) that exits from joints. Width of view about 1.5 m. **f** Detail of preceding photograph shows layer of breccia cemented laterally to the overhanging surface of the boulder. In the field, breccia induration decreases from the boulder surface outwards into un-lithified rockslide material over a distance of about 20 cm. The outwards decrease in lithification corresponds to an overall decrease of both cementation and the number of diagenetic phases recorded in thin sections. *Pen* for scale is 14 cm

Relative to typical values of 170–220 µS/cm for springs from the Hauptdolomit (without Seefeld Formation) in the wider environs (Probst et al. 2003), this is up to more than 100 micro-Siemens higher. In general, in the scarp area of rockslides, waters of elevated electrical conductivity are common (e.g. Weidinger et al. 1996; Weidinger 1998). Springs emerging from the Fern Pass rockslide deposit typically show conductivities of 380–420 µS/cm, i.e. still higher values than the springs from adjacent bedrock units. The relatively high conductivities of rockslide-emergent springs probably result from dissolution of the carbonate-lithic matrix. For the rockslide deposit, high contents in thorium and uranium are indicated by elevated ^{222}Rn of spring waters. On Fern Pass, Radium Spring records up to 185 Bq/l emitted from ^{222}Rn; this is among the highest radioactivities of spring waters in the Tyrol (Krüse 1926, 1937, 1940). Of all springs measured in the Fern Pass area, Radium Spring also showed the highest conductivity: 575 µS/cm. Because the half-live of ^{222}Rn is 3.82 days, to keep this element in measurable concentrations requires swift groundwater flow (Goldbrunner and Zötl 1993). The elevated contents of Rn, Th and U probably stem mainly from the black shales and organic-rich carbonates of the Seefeld Formation. The average uranium content of the Seefeld Formation is about 17 ppm, with maxima of 47.0 ppm associated with the black shales and organic-rich dolostones (Köster et al. 1989). Liberation of thorium and uranium can be attributed to intense fragmentation of rocks during the sturzstrom event (cf. Gundersen et al. 1992; Purtscheller et al. 1995). An elevated content of the rockslide mass in free thorium and uranium is also supported by high

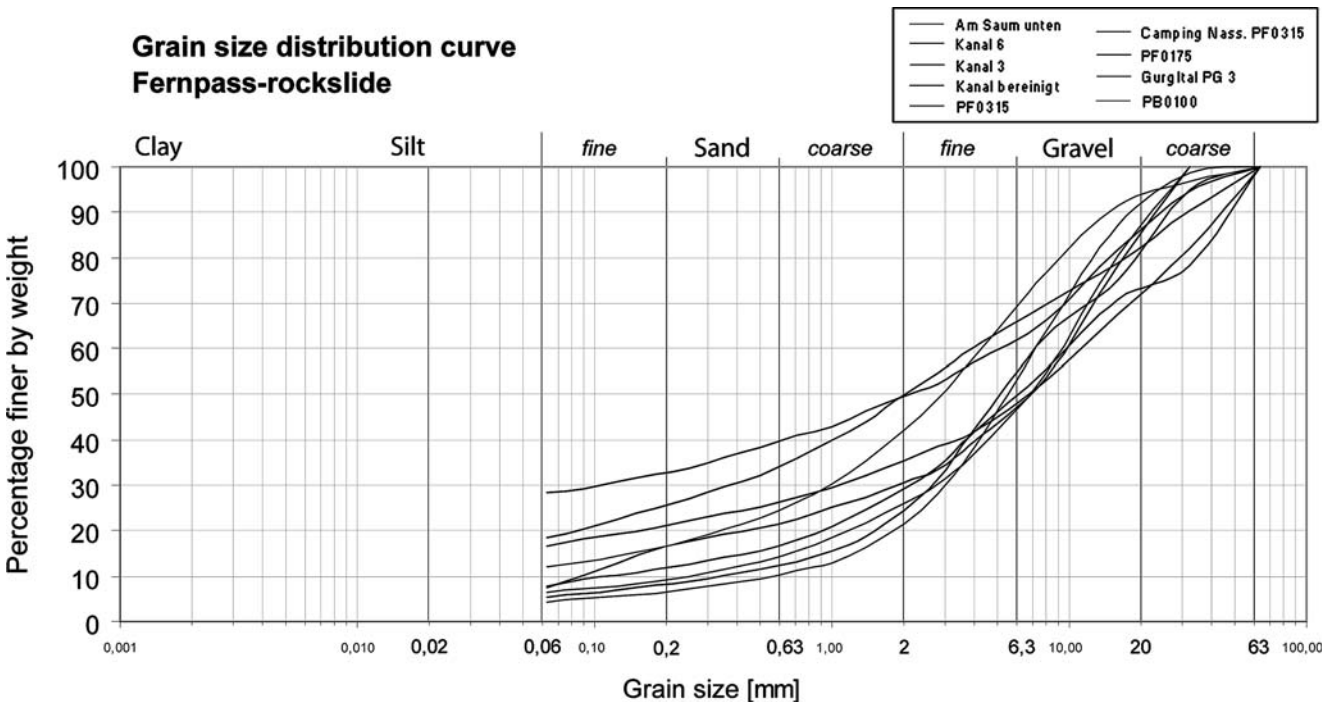

Fig. 3 Grain-size distribution in the fraction 0.063–63 mm of nine samples from the matrix of the rockslide. Note similar shapes of grain-size distribution curves. Size distribution of the silt- to clay-sized fraction has not been subdivided. The content of silt- to clay-sized material ranges between 5% and 28%

Table 1 Sample sites of lithified rockslide debris (breccias) and tufa limestones. Geographic co-ordinates according to Austrian Grid (Bundesmeldenetz), meridian M 28

Sample	Longitude (W)	Latitude (N)	Altitude (m)	Sample type, location	Exposition
PF 300	186,510	244,165	940	Breccia, apical part of southern flank of toma	Southern
R	187,300	245,500	980	Breccia, middle part of southern flank of toma	Southwestern
K	186,655	243,960	900	Breccia, excavation pit at eastern base of toma	Eastern
FP 1	187,515	245,800	950	Tufa at base of boulder, near base of toma	Southern

contents of these elements within the age-dated aragonite cement described below.

In the proximal to medial part of the rockslide, scattered angular boulders up to about 10–15 m in exposed diameter project above ground. In the upper to middle south-facing slope of toma hills, along the southern flank of projecting boulders more than about 4 m in exposed width, at several locations (some shown in Fig. 1), adjacent to boulders, carbonate-cemented breccias were found that are the subject of this paper. The breccia clasts are the same lithologies as the rest of the rockslide mass. In the breccias, no indication for aquatic transport was observed, such as bedding or stratification or sorted beds or strata. In addition, no evidence was found that the breccias represented small talus wedges that accumulated along boulder flanks subsequent to the rockslide. Instead, aside of minor modifications of fabric in a vadose diagenetic environment, the clast inventory of these breccias represents the pristine rockslide material.

Methods

Three locations of carbonate-cemented breccias and one of tufa limestone were sampled (Fig. 1; Table 1). Cut-and-polished rock slabs and 14 thin sections 4×6 cm in size provided documentation of facies and cementation of breccias and tufas. Polished thin sections were investigated under cold cathodoluminescence and epifluorescence. For measurement of stable isotopes of oxygen and carbon of the U–Th age-dated cement, five cleaned and polished rock slabs (i.e. different subsamples from the same field site) were excavated with a dental drill (diameter 0.5 mm). The stable isotope contents [Vienna Peedee Belemnite (VPDB) standard] were measured on a Finnigan DeltaPlusXL mass spectrometer connected with a gas bench (see Spötl and Vennemann 2003, for method). For U–Th age dating, the cement was sampled with a microdrill under the microscope. Organic material was removed physically as far as possible. Samples were spiked with a mixed ^{236}U–^{229}Th spike and dissolved in HNO_3, whereafter remaining organics were dissolved with $H_2O_2 + HNO_3$. U and Th separation was done using 2-ml anion resin (Dowex 1×8) and HNO_3 in early series, and 0.5 ml Eichrom U-Teva resin for later series. U and Th analyses were performed separately on an Nu-Instruments multi-detector inductively coupled plasma (MC-ICP) mass spectrometer. ^{236}U and ^{234}U were measured in separate electron multipliers (static mode). Thorium measurements were done in dynamic mode by alternate measurement of ^{230}Th and ^{229}Th in the same multiplier. For thorium measurements, to control electron multiplier gain, the MOSS (Be Inhouse) standard was used. For gain calibration of U, the National Institute of Standards in Technology (NIST) U 050 standard was applied. In our samples, the main difficulty in precise measurement of the $^{230}Th/^{232}Th$ ratio resulted from low ^{230}Th concentrations because of both, low uranium content and low age versus detrital ^{232}Th contamination. For carbonates, $^{230}Th/^{234}U$ disequilibrium fractionation provides the basis for age dating (Mallick 2000). To correct for detrital contamination, the main problem in age dating authigenic carbonates (Kaufman 1993; Debaene 2003), we chose the isochron method with several sub-samples (cf. Ludwig and Titterington 1994; Lin et al. 1996; Frank et al. 2000; Geyh 2001, 2005; Mallick and Frank 2002) plotted in $^{230}Th/^{232}Th$ versus $^{234}U/^{232}Th$ activity diagrams (Rosholt 1976) (Rosholt diagrams). In the Rosholt diagrams, the plotted $^{230}Th/^{232}Th$–$^{234}U/^{232}Th$ activity ratios of sub-samples then are connected, or approximated, by a regression line that can be considered as an isochron. At least three sub-samples must be measured to deduce an isochron line. In systems that were closed after crystallisation, the precision of an isochron age should increase with increasing number of (sub)samples. Under diagenetic conditions, however, partial re-opening of the system is common; hence, mere increase of sub-sample number does not necessarily increase the precision of calculated ages. To better recognise (sub)samples that potentially were subject to re-opening, the measured contents in thorium and uranium isotopes were plotted into a "closed-system check" (CSC), i.e. into a diagram of

$^{230}Th/^{238}U$–$^{234}U/^{238}U$ activity ratios. The CSC is a semi-quantitative test for whether the system was closed or open after crystallisation. In systems that are genetically related and remain closed after crystallisation, except for differences in $^{230}Th/^{238}U$ activity ratios before closure, the activity ratios of (sub)samples cluster and, in particular, $^{234}U/^{238}U$ ratios are similar. In the CSC, the absolute values of activity ratios are irrelevant. The CSC is based on the confidence that within a (sub)sample set, most (sub)samples will not have been subject to re-opening. Sub-samples that suffered post-closure overprint (e. g. because of partial re-opening) plot off the cluster and hence are better recognisable. In the Rosholt diagrams, the slope of the regression line among the measured values of $^{230}Th/^{232}Th$–$^{234}U/^{232}Th$ activities (of sub-samples) yields *corrected* activity ratios; these corrected ratios are used to calculate the absolute age. For age calculation, the corrected activity ratios were fed into a U–Th disequilibrium age calculation program (Visual Basic, written by Jan Kramers, unpublished, according to the equation of Kaufman and Broecker 1965).

Results

Field presence of breccias and tufa limestone

As mentioned, in the upper (sample location PF) to middle (sample location R) (see Fig. 1) part of the southern flanks of toma hills, breccias lithified by carbonate cements were observed. The breccias are present in the immediate southern understory of boulders and/or are cemented to the vertical to overhanging flanks of boulders. The breccias comprise decimetre-sized patches and "crusts" up to about 20- to 30-cm thick in contact to the flanks and along the base of projecting boulders (Fig. 2c–f). In all observed cases, the subaerially exposed width of boulders associated with breccias is about 4 m at least; for boulders of smaller exposed size, no breccias were observed. Most breccias are present in the medial portion of the southern rockslide branch between the village Nassereith and Fern Pass (cf. Fig. 1). Laterally outwards and downwards from the boulders and their associated breccias, cementation rapidly tapers out, and the deposit is unlithified. Fresh man-made outcrops of location K (Fig. 2c), situated near the eastern base of slope of a toma hill, indicate that, aside of cementation, no marked difference is obvious between clast fabrics of cemented and non-cemented portions of the rockslide. Because of both the lateral variability and small size of the breccia patches, the number and type of diagenetic phases as identified in thin sections is variable (see below). In the portion of breccia patches adjacent to boulders, cementation of breccias is most pronounced, diagenetic successions are most complete and variegated and carbonate cements (including the age-dated aragonite) are best developed (Figs. 2e and f, 4a). Both outward/downward and laterally off the boulders, in the breccia patches and crusts, the number of petrographically identifiable diagenetic phases decreases. In addition, in south-facing positions below overhangs of projecting boulders, ledges of porous tufa limestone devoid of or poor in lithoclasts are present. Overall, at Fern Pass, this type of tufa limestone is less common than the breccias. A large boulder with a tufa ledge underneath its overhanging, southern face (Fig. 4b), is capped by an interval of soil that is vegetated by bushes and small pine trees.

Petrography of breccias

Both the degree of lithification and the number of diagenetic phases, as distinguished by microscopy, fade outwards from the contact of the breccias with the boulders. The most distinct variability of diagenesis in thin sections is that outwards, away from boulder surfaces. Outwards, the overall disappearance of diagenetic phases takes place along a gradient of a few centimetres to about 25–30 cm and thus can be obvious also in individual thin sections and is always obvious in successive thin sections out from boulder surfaces. In addition, a lateral variability of diagenetic records is indicated parallel to local boulder surfaces. On the scale of thin sections and cut slabs, however, this variability is less clear cut than that in the outwards direction. Finally, in addition to these variations, different breccias from different locations show distinct diagenetic successions. Hereunder, three types of diagenetic succession are distinguished, from simple to more complicated, that correspond to breccias of different sampling sites.

Type 1 diagenetic succession In samples from an excavation pit at location K (see Fig. 1), the most complete diagenetic successions adjacent to boulders include thin isopachous to slightly mammillary crusts of micrite overlain by an isopachous fringe of dog-tooth spar. Remnant pore space is open (Fig. 4c). Outwards and downwards from the boulder surface, the fringe of dog-tooth spar thins and tapers out within a few centimetres, and lithification is only by crusts of micrite (Fig. 4d). Still farther out, the micrite crusts becomes patchy and finally vanishes, and the deposit is unlithified.

Type 2 diagenetic succession At location R, samples from the medial part of south-facing slopes of tomas

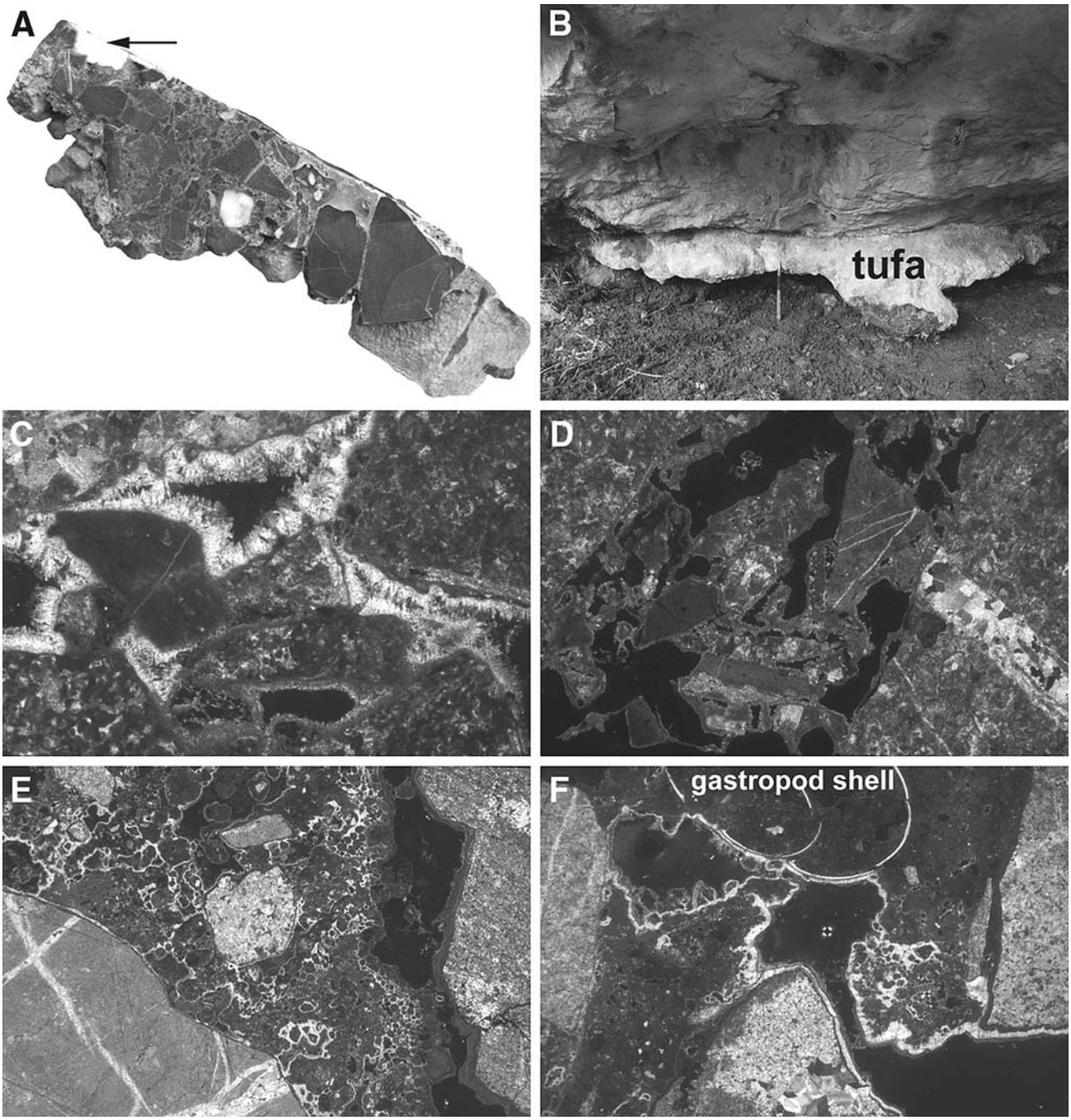

(see Fig. 1) are lithified by an isopachous to mammillary crust of micrite on lithoclasts. In larger interstitial pores, the micrite crusts are overlain by a porous, very poorly sorted, grainstone to, locally, packstone of soil peloids (Fig. 4e). The soil-peloidal grainstone is cemented by isopachous fringes of finely crystalline cement with an indistinct radial-fibrous fabric. The radial-fibrous cement, in turn, is locally overlain by a fringe of micrite and/or another thin fringe of cement with a faint radial-fibrous fabric (Fig. 4e). In one thin section of this location, a Holocene gastropod shell is present (Fig. 4f); under crossed nicols, the shell shows a sweeping extinction characteristic of aragonitic preservation. Another sample of the same location R represents a crust about 6-cm thick of breccia cemented onto a boulder. The clasts of this breccia are supported by a matrix of faintly non-gravitationally (subparallel to the steep boulder surface) layered grainstone to fine-grained rudstone. The components of the grainstone to rudstone are soil peloids and coarse sand to fine gravel-sized, angular and

◀ **Fig. 4** Field presence and petrography of rockslide breccias. **a** Cut slab of breccia shown in Fig. 2e, f. The upper side of the slab was situated directly along and cemented to the overhanging surface of the boulder (Fig. 2f). The white patch (indicated by *black arrow*) is a larger area of aragonite cement 1 (cf. Table 2) that has been age dated by the Th–U disequilibrium method. Aside from aragonite cement 1, the remainder of the breccia is mainly lithified by crusts of micrite and isopachous fringes of calcite spar. Note that some of the lithoclasts show rounded edges. **b** Protruding ledge of porous tufa limestone formed in the shaded angle between an overhanging, south-facing boulder surface above and vegetated soil below (sampling location FP 1; see Fig. 1). The vegetation here consists of moss tufts and stout grass shoots (vegetation was removed for photograph). The present top of the soil is a few centimetres below the base of the tufa ledge. *Pen* for scale is 14 cm. **c** Breccia from sampling location K (see Figs. 1, 2b). Detail of sedimentologically uppermost portion of breccia sample. Lithoclasts of peloidal grainstone are overlain by thin isopachous to mammillary crusts of micrite to carbonate-lithic wackestone. Above, an isopachous fringe of dog-tooth spar is present. *Black*: open pores. Crossed nicols. Width of view 6.5 mm. **d** Same breccia sample as shown in preceding photograph. Detail of sedimentologically lowermost portion. Down to the photographed position, the isopachous fringe of dog tooth spar obvious in the topmost part (see **c**) becomes progressively thinner and of smaller crystal size (not because of truncation by dissolution), and the breccia is exclusively lithified by a fringe of micrite cement. The micrite cement is in physical continuity with the micrite cement fringe that, in the topmost portion of the same sample, underlies the isopachous dog-tooth spar. *Black*: open pores. Crossed nicols. Width of view 6.5 mm. **e** Breccia of location R (cf. Fig. 1), sample R1. The breccia shows a clast-supported fabric, with the pore space filled by very poorly sorted peloidal grainstone to fine-grained peloidal rudstone. *Black*: open pores. Crossed nicols. Width of view 17 mm. **f** Breccia of location R (cf. Fig. 1), sample R1. Dolosparstone clasts of Hauptdolomit unit, patch of peloidal packstone to grainstone, and gastropod shell filled by porous peloidal grainstone to packstone. Note the isopachous fringe of cement. *Black*: open pores. Crossed nicols. Width of view 17 mm

embayed nodules of carbonate-lithic wackestone to lime mudstone (Fig. 5a). In the portion of the sample adjacent to the boulder surface, the grainstone to fine-grained rudstone is lithified by a thin isopachous fringe of cement. The cement, in turn, is overlain by lime mudstone that largely fills the remnant pore space. Dissolution pores within the lime mudstone, in turn, are overlain by another thin fringe of cement (Fig. 5a). Farther off the boulder surface, the same matrix-supported breccia sample contains micrite-encrusted moss relicts and phytomoulds (e. g. after moss stems), but still contains floating clasts of Seefeld Formation (Fig. 5b). This latter type of limestone is transitional between breccias and "pure" tufa limestone. At location R, however, no pure tufa has been identified.

Type 3 diagenetic succession The most complex diagenetic succession is recorded in samples of location PF (see Fig. 1), where the age-dated aragonite cement comes from. Near the southern-exposed apical area of a large toma hill, several boulders associated with breccias are present. In thin sections of breccias, up to eight stages of diagenesis can be distinguished (see Table 2). Again, the most complete diagenetic successions are present near the overhanging surface of the boulder (Figs. 2f, 5c) and taper out and become more incomplete outwards from the boulder surface. In all thin sections, the first phase of diagenesis is represented by a very thin, isopachous to patchy, non-gravitational crust of micrite. Adjacent to the boulder, this micrite crust is overlain by a fringe up to about 8-mm thick of aragonite cement with well-preserved radial-fibrous structure (Fig. 5d, e). The preservation of this cement fringe as aragonite has been verified by X-ray diffraction. This aragonite fringe is the thickest of all cements in the samples from this location and has been age-dated with the U–Th method. Subsequent to precipitation of the age-dated aragonite cement 1 (see Table 2), the diagenetic history is characterised by two phases of distinct dissolution (affecting also the age-dated aragonite cement; Fig. 5f). The phases of dissolution changed with precipitation of micritic cement, of scalenohedral calcite and, locally, with precipitation of a thin fringe of younger aragonite cement (Fig. 6a, see also Table 2). At the same sampling location PF, less complicated diagenetic successions consist of dissolution truncation and lithification of a matrix of carbonate–lithic wackestone to carbonate–lithic siltite overlain by an isopachous fringe of dog-tooth spar (Fig. 6b, c). The thin sections from location PF showed no cathodoluminescence. Similarly, epifluorescence microscopy had very low yield and did not indicate additional diagenetic phases or dissolution surfaces within cement fringes. In the age-dated aragonite cement 1, of fifteen stable isotope measurements of oxygen and carbon, the oxygen isotope values range from −7.4‰ to −6.8‰ $\delta^{18}O_{(VPDB)}$; the carbon isotope values range from 7.5‰ to 13.3‰ $\delta^{13}C_{(VPDB)}$ (Table 3).

Petrography of tufa limestone

In addition to the breccias, along the base of a south-facing vertical to overhanging flank of a large boulder, ledges and bumpy crusts to protruding patches up to about 10-cm thick and about 25-cm long of tufa limestone are present (Fig. 4b). In thin section, the tufa consists of micrite, micropeloids, peloids and crusts of calcite cement; the tufas are rich in open fenestral pores of unknown origin, and in open phytomoulds after moss stems. Both the moss stems and other phytodetritus became encrusted by fringes of calcite cement (Fig. 6d). Above the cement fringes, fringes and patches composed of micrite and/or of micropeloidal grainstone to

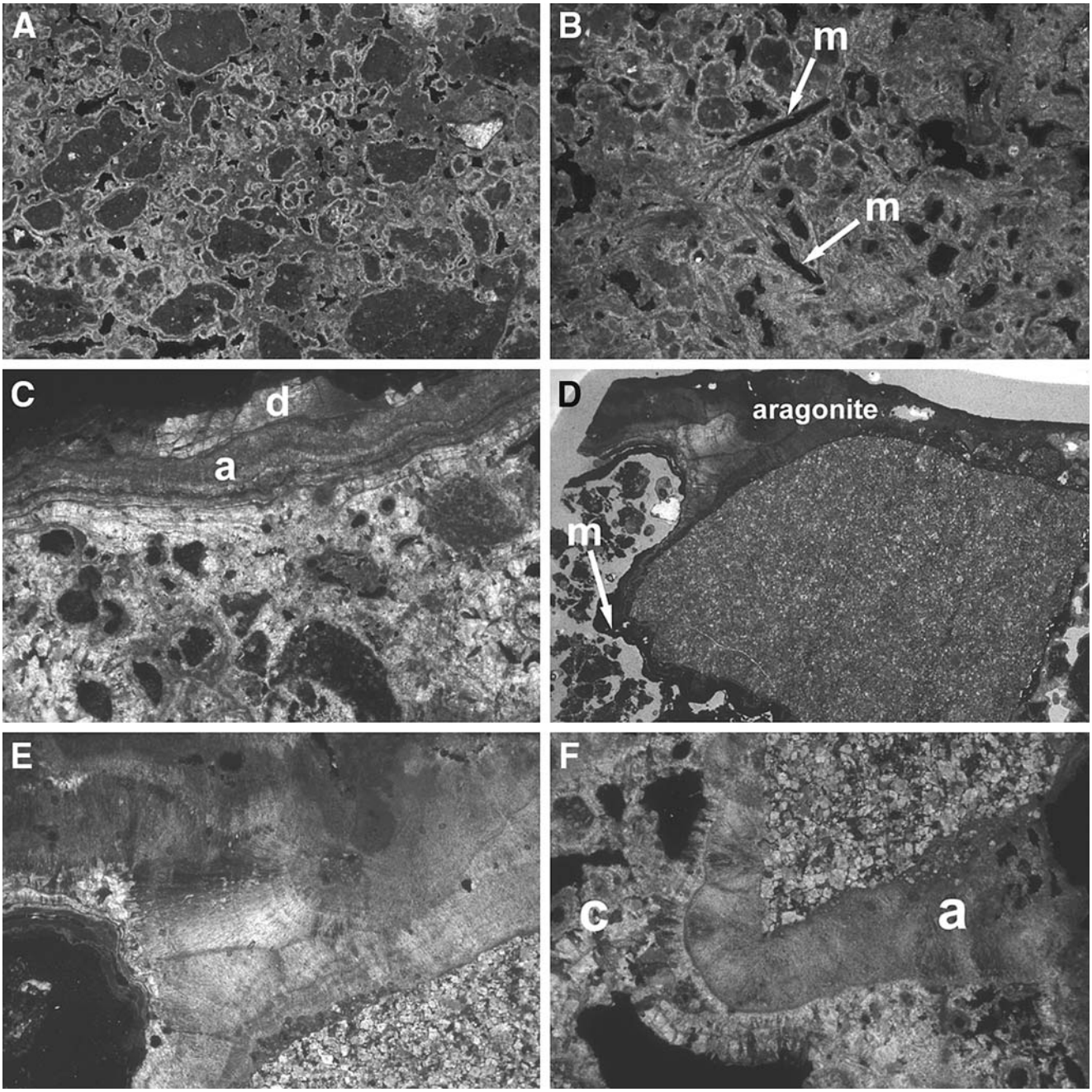

packstone are present. The remnant pore space in fenestrae may be coated by a very thin isopachous fringe of calcite with elongate radial-fibrous crystals.

Thorium–uranium dating

Because aragonite cement 1 (cf. Table 2) can be readily located both on polished slabs and in thin section, and because of its position early in the diagenetic succession, this cement has been chosen for age dating. The U–Th age is 4,150 ± 100 years (Fig. 7a). The uranium content of aragonite 1 ranges between 95 and 179 ppm (Table 4). In the closed system check, the activity ratios of all samples for U–Th age determination plot into a very dense cluster (Fig. 7b); this indicates that the system remained closed after aragonite precipitation.

Interpretation

The association of the described breccias and tufa limestones to the immediate contact zone with boulders suggests a link between calcium carbonate precipitation and presence of boulders. A causal connection

◀ **Fig. 5** Petrography of rockslide breccias. **a** Breccia of location R (cf. Fig. 1), sample R2. Matrix-supported breccia adjacent to a boulder. Detail of lower/inner part (close to the boulder surface) of sample. Very poorly sorted peloidal grainstone to, locally, diagenetic packstone. This matrix supports gravels of Hauptdolomit. In the matrix, the large peloids show an highly irregular shape and consist of lime mudstone to carbonate-lithic wackestone. The peloids are coated by a thin fringe of carbonate cement. The remnant pore space between the cement fringes is filled by micrite (diagenetic packstone); the micrite, in turn, is riddled by fenestral pores (*small black patches*). These pores, in turn, may be lined by a very thin fringe of calcite cement. Crossed nicols. Width of view 8.5 mm. **b** Detail of upper/outer part (more distant relative to boulder surface) of same sample R2 than shown in preceding photo. Very poorly sorted peloidal grainstone. The grainstone here contains intercalated patches with remnants of moss plants that became encrusted by calcite cement; the moss stems are preserved as open phytomoulds (*m*). Aside of the phytomouldic pores, fenestral dissolution pores are present. *Black*: open pores. Crossed nicols. Width of view 6.5 mm. **c** Breccia of location PF 300 (cf. Fig. 1). Diagenetic succession of U–Th age-dated sample. On the *upper margin* of photo, a layer of saddle dolomite (*d*) is present that represented part (probably a vein) of the boulder of Hauptdolomit the breccia was cemented to (cf. Fig. 2f). The saddle dolomite is overlain by a very thin fringe of micrite that, in turn, is overlain by the fringe of Th–U age-dated aragonite 1 cement (*a*) (see Table 2). The aragonite crust is truncated and is overlain by isopachous calcite cement with intercalated thin layers of micrite. Above this calcite/micrite layer, in the *middle and lower part* of the photograph, a grainstone is present that consists mainly of subcircular mouldic pores (*black* in photo; probably phytomoulds) and of clasts of micropeloidal grainstone, coated by a fringe of calcite spar. Crossed nicols. Width of view 6.5 mm. **d** Breccia of location PF 300 (cf. Fig. 1). Sample PF 300E of breccia with age-dated aragonite cement 1. The upper side of this sample was cemented to a boulder, as shown in Fig. 2F. The lithoclasts of the breccia are dolosparstones of the Hauptdolomit unit. In the *upper part* of the photo a thick botryoidal fringe of aragonite (aragonite cement 1; see Table 2) is obvious. The aragonite cement is truncated and overlain by a crust composed mainly of micritic cement and very thin isopachous fringes of calcite cement. Below the lithoclast, this composite cement crust shows pendant mammillary fabrics (*m*). Parallel nicols. Width of view 17 mm. **e** Detail of **d**. Shows well-preserved radial-fibrous structure of the age-dated aragonite cement 1 and its truncation towards the open pore. Dolosparstone in *lower right* part of photo is clast of Hauptdolomit. Crossed nicols. Width of view 6.5 mm. **f** Breccia of location PF 300 (cf. Fig. 1), sample PF 300B/1. The coarsely crystalline dolosparstone in *upper right* is a clast of Hauptdolomit. The clast is overlain by an isopachous fringe of aragonite (labelled *a*, aragonite cement 1). The aragonite, in turn, is truncated, and became overlain by a fringe of prismatic calcite cement that shows faint growth lines subparallel to its surface. *Black* open pores. Crossed nicols. Width of view 17 mm

between boulders and breccias is also indicated by the decrease, outwards from the contact zone, in overall thickness of cement and number of diagenetic phases. The breccias and tufas are present closely above to below the intersection of the exposed boulder surface with soil-covered terrain. Furthermore, the observation that breccias and sizeable patches of tufa limestone were observed only in association with boulders more than about 4 m in subaerially exposed width indicates that there is a link between exposed boulder surface size and cementation in their contact zone, near and closely below the intersection of the boulder surface with the soil. These observations are integrated into a meteoric diagenetic system wherein water runoff from boulder surfaces results in small-scale, fluctuating, vadose to essentially phreatic diagenetic environments (micro-phreatic environments) at the loci where surface runoff from boulders seeps into the terrain within which boulders are embedded (Fig. 8).

The calcium carbonate for breccia cementation and formation of small tufa ledges probably stems largely from dissolution of the fine-grained matrix of the rockslide. The presence of vegetated soil atop boulders and the observation that water percolates out of joints of larger boulders, however, suggests that minor dissolution of the boulders themselves may have contributed to calcium carbonate precipitation. Meteoric water percolating through soil becomes enriched in dissolved CO_2 and organic acids, which, in turn, increases the potential of the water for carbonate dissolution (cf. Egli and Fitze 2001). Upon soil-modified waters seeping through joints, carbonate is dissolved, and after exit of these waters from the boulder into the adjacent rockslide deposit, contributes to oversaturation for calcium carbonate in pore waters. This may explain why breccias and tufas have been observed only in association with boulders at least about 4 m in subaerially exposed size. Even today, however, after more than 4,000 years of meteoric vadose leaching and matrix elutriation, the shallow portions of the rockslide body contain a sizeable percentage of silt- to clay-sized carbonate-lithic matrix of dolomite and limestone. If just leaching of the rockslide matrix by soil-modified meteoric waters were decisive in cementation, the entire rockslide should be cemented in its shallow portions; this is not the case. As mentioned, all springs emerging from the rockslide show elevated electrical conductivity (this study). This indicates that these waters contain a relatively high percentage of dissolved ionic substances, probably mainly Ca^{2+} and HCO_3^- from dissolution of the fine-grained matrix of the rockslide. The lack of near-surface cementation of the entire rockslide mass and absence of tufa downstream rockslide-emergent springs suggest that the diagenetic system along boulder surfaces is controlled by a *balance* between water supply plus retention and attainment of sufficiently high supersaturation for calcium carbonate for effective precipitation. The function of boulders more than about 4 m in subaerially exposed width is therefore to focus a sufficiently large amount of water runoff along their surface and to delay downwards pore-water

Table 2 Diagenetic phases identified in samples of PF 300

Diagenetic stage features	Diagenetic phenomenon	Interpretation, diagenetic environment	Remarks
Stage A Micrite crust	Clasts coated by (laminated) crust and non-gravitational patches of micrite. Micrite may contain lithic silt to sand (mudstone to wackestone to packstone texture), and/or alveolar structures	Cementation in vadose zone Precipitation of micritic cement with admixed carbonate-lithic silt to sand Alternative: infiltrated matrix adherent to clasts	In all thin sections Locally absent because of original absence and/or because of later dissolution (stage C and later dissolution phases)
Stage B Aragonite 1 (U-Th age: 4,150 ± 100 years)	Isopachous crusts and botryoids of radial-fibrous aragonite cement. Locally, entire interstitial pore space filled by aragonite.	Aragonite cementation under micro-phreatic conditions.	Locally absent mainly because of subsequent dissolution (stage C) Dissolution after aragonite precipitation recorded in all thin sections.
Stage C Dissolution phase 1	Aragonite 1 overlain along sharp, irregular boundary by other cements	Dissolution of aragonite cement. Return of vadose conditions, and/or switch of pore water to aragonite undersaturation.	This phase *discretely* recorded only where aragonite is overlain by cements of stage D.
Stage D Calcite spar	Precipitation of isopachous crusts of scalenohedral and prismatic calcite spar.	Calcite precipitation under micro-phreatic conditions.	Locally absent because of subsequent dissolution (stage E and succeeding stages).
Stage E Dissolution phase 2	Truncated cements (stages A, B, D) overlain by cements of stage F.	Dissolution of all previous fabrics Return of vadose conditions, and/or switch of (phreatic) pore water to undersaturation for all polymorphs of calcium carbonate.	This phase *discretely* recorded only where aragonite and/or calcite are overlain by cements of stage F.
Stage F Aragonite 2, micrite, soil peloids	Isopachous crusts of aragonite cement and/or of crusts (locally microstromatolithic) of micrite and clotted micrite with soil peloids mm- to cm-sized patches of soil-peloidal grainstone cemented by fine-grained aragonite cement	Rapid switches between micro-phreatic conditions (aragonite 2) and vadose conditions (micritic cements), local formation of mm-sized patches of grainstone of soil peloids cemented by very-fine-grained aragonite	Record of stage F locally absent
Stage G Micrite crusts	Laminated crusts of micrite. Crusts thicken towards sedimentological bottom of samples Near sedimentological bottom: crusts may be present in geopetal pendants bon clasts, and typically directly overlie clasts	Terminal phase of dissolution and micritic cementation	Stage G present in all thin sections. Becomes more distinct and the only diagenetic phase towards the sedimentological bottom of samples.
Stage H Infiltrated soil	Remnant pores filled by soil rich in micritic soil peloids	Infiltration of soil in vadose environment	-

percolation long enough to allow for diagenetic products to form. The observation of breccias and tufas along the southern to eastern sides of toma hills may suggest that increased evaporation helped to concentrate "normal" pore waters to supersaturation for calcium carbonate. Along boulder surfaces facing south, evaporation of waters seeping over the surface can presently be observed (Fig. 2e). In addition, the soil along the southern side of boulders is subject to increased evaporation. That evaporation is important in producing supersaturation is further suggested by the stable isotope values of the age-dated aragonite cement. In particular, the very high positive carbon isotope values indicate that the aragonite-precipitating waters were strongly conditioned by kinetic effects, such as evaporation. In summary, precipitation of the meteoric vadose and phreatic cements took place in a diagenetic window wherein both supersaturation of soil-modified evaporatively concentrated waters was high and retention of oversaturated pore waters was long enough to allow for cement precipitation.

In the breccias, the non-laminated to laminated local mammillary crusts and pendants of micritic cements probably formed when the diagenetic environment was vadose. The origin of crusts and irregular patches of carbonate-lithic wackestone to packstone (see Fig. 6b)

Table 3 Stable isotope values of age-dated aragonite cement 1 in sample PF 300 (cf. Table 2)

Sample	δ 13 C (‰ VPDB)	δ 18 O (‰ VPDB)
PF 300-1	12.15	−6.90
PF 300-2	11.59	−6.88
PF 300-3	7.87	−7.10
PF 300-4	13.29	−6.82
PF 300-5	11.09	−7.07
PF 300-6	7.50	−7.37
PF 300-7	12.59	−7.11
PF 300-8	12.59	−7.05
PF 300-9	12.01	−7.02
PF 300-10	9.62	−7.13
PF 300-11	11.54	−7.13
PF 300-12	12.32	−6.81
PF 300-13	11.83	−7.05
PF 300-14	11.26	−7.18
PF 300-15	11.38	−7.02
Mean	11.14	−7.07
Minimum	7.50	−7.37
Maximum	13.29	−6.81

VPDB Vienna Peedee Belemnite

is less straightforward to interpret. In the vadose zone of recent unlithified coarse-grained deposits of the NCA, such as talus slopes, clasts often are coated by infiltrated carbonate silt to mud with admixed sand grains (own observations). Partial dissolution and/or lithification of such matrices may result in a "pseudo-cement" (cf. Elbracht 2002). Alternatively, calcifying biofilms around clasts may have trapped infiltrating material. More-or-less calcified biofilms around clasts were observed in artificial outcrops in the vadose zone of recent soil-covered talus slopes of the NCA (Fig. 6e). The fringes of aragonite calcite cements, by contrast, record essentially phreatic diagenetic conditions that were limited to the immediate contact zone near boulder surfaces. In Quaternary deposits of the NCA, isopachous carbonate cements (calcite, aragonite) that record similar, essentially phreatic, diagenetic environments are common in coarse-clastic deposits situated in subaerial settings of overall vadose character, such as the deeper portions of talus slopes and talus slopes and that became lithified immediately below springs (Sanders 2001; Ostermann 2006; Ostermann et al. 2006). For the breccias of the Fern Pass rockslide, the diagenetic environment adjacent to boulders thus fluctuated between essentially phreatic and vadose and between supersaturation and undersaturation for aragonite and/or calcite.

Meteoric cements of Quaternary coarse-grained deposits (talus breccias, pebbly alluvium) of the NCA commonly show total uranium contents between 0 ppm and about 50 ppm (Ostermann 2006). The uranium content of 95–179 ppm of the age-dated Fern Pass aragonite 1 thus is exceptionally high and probably results from intense fragmentation of the black shales and organic-rich carbonates of the Seefeld Formation involved in rocksliding. The high U-concentration of the aragonite fits well with the mentioned ^{222}Rn-produced radioactivity of rockslide-emergent springs. In the closed-system check, activity ratios of the five analysed sub-samples of Fern Pass plot into a very tight cluster. Similarly, the deviation of sub-samples from the (isochron) regression line is very small. Together, the high uranium content of the aragonite, the dense clustering of activity ratios and the good fit of the isochron line all indicate that the system was closed after precipitation and that the deduced age of 4,150 ± 100 years is of high accuracy. The U–Th age of the aragonite fits well with ^{14}C ages of wood fragments from rockslide-dammed torrent deposits. The wood fragments indicate an age between 3,080 and 3,380 cal. years BP. The age of the backwater succession base, however, is not yet established (Prager 2005). Two ^{36}Cl exposure ages of slide planes of the rockslide scarp were determined as 3,400 ± 900 years and 4,800 ± 1,200 years, with a mean of 4,100 ± 1,300 years (Prager et al. 2006a). This indicates that the age-dated aragonite cement 1 precipitated shortly after rockslide deposition, i.e. cementation age represents a good proxy age of the failure event.

Discussion

In the Quaternary of the Alps, aragonite cement is fairly common, for instance, in spring tufas (Sanders et al. 2006a, b) and in some active ground-water flow systems that precipitate speleothems (Spötl et al. 2002). In the present case, precipitation of aragonite instead of calcite may result from Mg^{2+} ions in pore waters (cf. Berner 1975; Laya et al. 1992) and/or from a high degree of supersaturation for calcium carbonate (cf. Chafetz et al. 1991). Immediately after the event, the rockslide sediment was rich in chemically reactive carbonate-rock flour produced by dynamic disintegration. On top of recent fresh rockslides, a veneer up to a few decimeters thick of abrasion-produced rock dust is common. In contact with meteoric waters undersaturated for calcium carbonate, part of the rock flour dissolved (dolostone rock flour in part may have dissolved incongruently), such that mainly calcium and a minor amounts of magnesium entered into pore waters. At *moderate* supersaturation for calcium carbonate, growth rates of both aragonite and

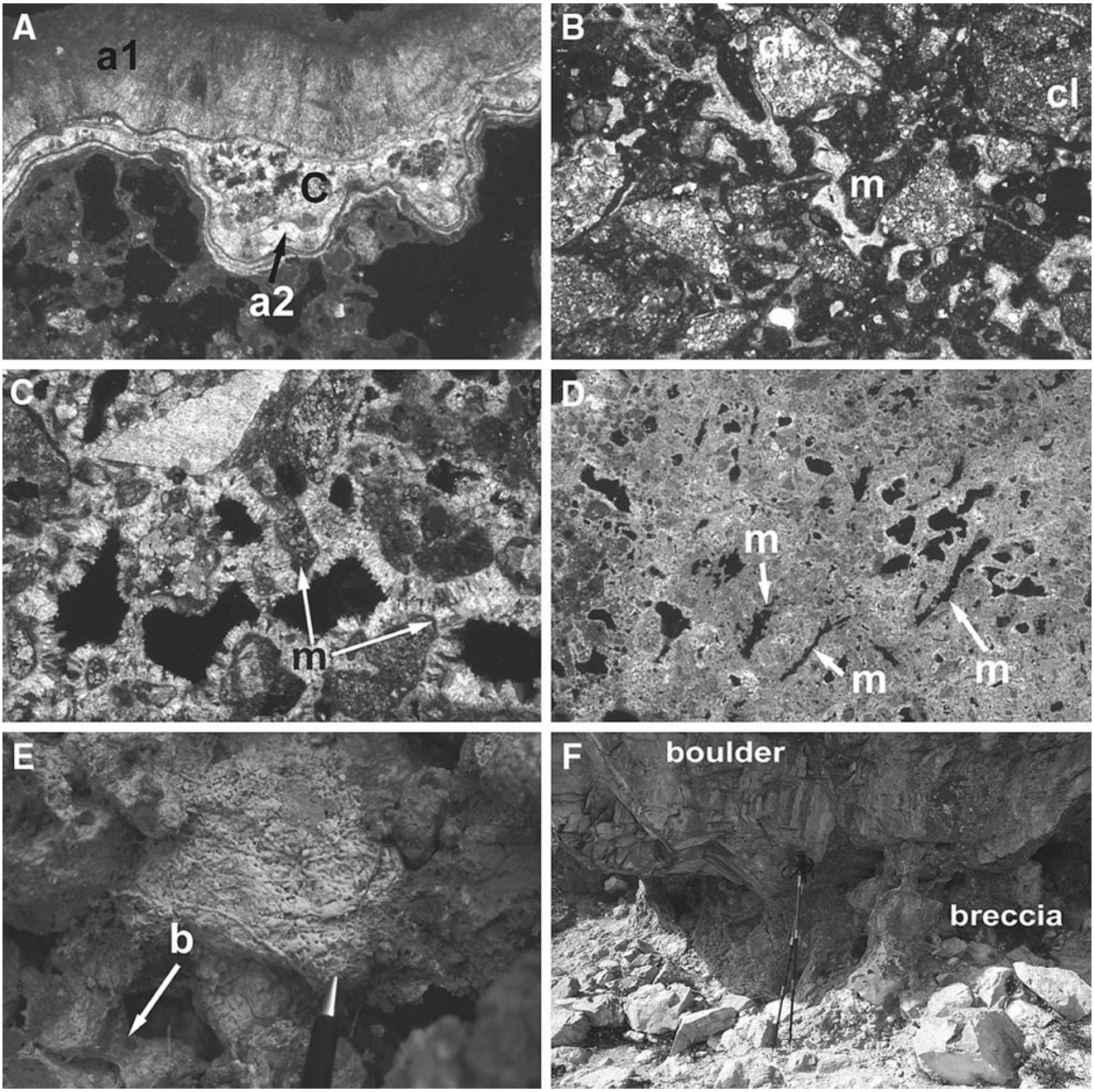

calcite depend on the ion product of calcium and bicarbonate (Gutjahr et al. 1996a). Without or at low concentrations of inhibitors such as magnesium, then, calcite precipitates. Because of dolostone dissolution, however, presence of Mg^{2+} ions may have prevented calcite precipitation and favoured crystallisation of aragonite (cf. Gutjahr et al. 1996b). In addition, at *high* supersaturation for $CaCO_3$ and ample supply of carbonate ions, even under absence of cationic inhibitors of calcite growth, aragonite growth is favoured (Meldrum and Hyde 2001). For the cement, potentially high degrees of supersaturation during mineral precipitation are supported by the stable isotope ratios of oxygen and carbon that record marked kinetic effects, probably due to water concentration mainly by evaporation (see above). In caves and fracture systems, aragonitic speleothems are considered as indicators of low availability of water (Railsback et al. 1994; Frisia et al. 2002; Spötl et al. 2002). At Fern Pass, therefore, both the presence of Mg^{2+} shortly after the rockslide event and high degrees of supersaturation of pore waters may have favoured early aragonite precipitation. High temperature during summer may have aided this development, but by

◀ **Fig. 6** Petrography of rockslide breccias and comparative counterparts. **a** Breccia of location PF 300 (cf. Fig. 1), sample PF 300B/2. Herein, the fringe of aragonite cement 1 (*a1*) is truncated and is overlain by a fringe of calcite spar (*c*). The calcite spar is present, or preserved, in a patch that is overlain by an isopachous layer of aragonite cement 2 (*a2*; cf. Table 2). Internally, aragonite 2 shows intercalated laminae of micrite. Aragonite cement 2, in turn, is overlain by a mammillary crust of micrite. The remnant pore space is partly filled by a highly porous aggregate of mixed peloidal/carbonate-lithic packstone and micrite. *Black*: open pores. Crossed nicols. Width of view 4.2 mm. **b** Breccia of location PF 300 (cf. Fig. 1), sample PF 300E. Lithoclasts (*cl*) of dolosparstone are from the Hauptdolomit unit. Between clasts, patches of irregular shape of a matrix (*m*) of dololithic wackestone to packstone are present. The patches or the clast surfaces, in turn, are overlain by an isopachous fringe of lucid prismatic calcite cement. Towards the sedimentologically lower part of the thin section, the isopachous calcite cement is locally absent because of gradual disappearance by thinning out. Parallel nicols. Width of view 8.5 mm. **c** Detail of the same thin section as in **b**. Dolosparstone clasts are cemented by thin fringes of varying thickness of micrite (*m*). Above, an isopachous fringe of prismatic calcite spar is present. Acute terminations of spar crystals locally are truncated by later dissolution. *Black*: open pores. Crossed nicols. Width of view 5.3 mm. **d** Tufa limestone from location FP 1 (see Figs. 1, 4b). The tufa consists of micrite, peloids and thin isopachous fringes of calcite cement present together in a fabric rich in fenestral pores (*black patches*). The fringes of calcite cement are present around fenestral pores that, by their shape and in some cases, can be identified as phytomoulds. The remnant pore space above the cement fringes is locally filled by lime mudstone and by peloids. *Arrows labelled m* indicate phytomoulds of moss stems. Crossed nicols. Width of view 14 mm. **e** Possible analogue to the formation of isopachous to mammillary crusts of micritic cement in coarse-grained deposits in the vadose diagenetic zone. Detail of man-made excavation into talus, about 2.5 m below talus surface (March 2005; Sankt Veit near Telfs, Tyrol, Northern Calcareous Alps). The talus clasts are coated by a white biomat (probably consisting of fungi and non-photosynthetic microbes) up to about 3-mm thick. The surface of the mat is soft and wet, but its understory is indurated. Physical removal of this biomat shows that the clast surfaces below are coated by a thin crust of micrite. *White arrow labelled b* shows bridge-like growth of biomat between clasts. *Pen tip* for scale is 8 mm in diameter. **f** Understorey of a boulder of Middle Triassic shallow-water limestone (Wettersteinkalk) on a Holocene talus slope (Halltal near Innsbruck, Tyrol, Northern Calcareous Alps) (Delago 2005). This boulder is one of a layer of scattered boulders up to about 10 m that was shed by a large rockfall, or rockfalls, onto the talus slope. Below the boulder, the relatively finer-grained talus material (sand to cobbles) is lithified by carbonate cements. The grey subvertical streaks on the boulder surface result from colonisation with lichens and cyanobacteria; these streaks represent preferred flow paths of water films sapping down the boulder during and after rains and upon snow melt. Note that the streaks on the boulder correspond with and extend into outweathering pillars of lithified breccia below. Width of view about 6 m

itself (i.e. not by its consequences, such as high evaporation), it is not required for aragonite precipitation; aragonite also precipitates in very cold settings as a result of high supersaturation (Aharon 1988; Sletten 1988). We found no evidence that cementation of the rockslide was active over larger areas. Otherwise, and given that cementation started soon after the event, the rockslide should be largely cemented by now. Therefore, the pace of cementation overall seems to have slowed with time after the event. Out of the contact zone of boulders, permeability—at least of the shallow levels of the rockslide deposit—is too high to allow for sufficient water retention and cementation.

Our concept of breccia cementation and tufa formation integrates type of deposit, position and exposition of boulders as well as their subaerially exposed width. The breccia cements formed in previously undescribed small-scale meteoric diagenetic systems controlled by the boulders, and fluctuated between essentially phreatic and vadose. Because there is no evidence for drastic climatic changes over the past $4{,}150 \pm 100$ years, and because the described diagenetic conditions do not seem very exceptional, one may expect to find similar breccias in other coarse-grained subaerial deposits. Preliminary observations from other areas in the western NCA strongly suggest that "boulder-controlled" small-scale meteoric cementation systems indeed may be common (Fig. 6f). It seems, however, that previously, cementation of rockslides has been mentioned only rarely and en passant. For the distal part of the Gohna Tal rockslide (Kumaon Himalayas, India) that consists mainly of carbonate rock clasts, breccias that formed "due to cementation by carbonate-rich waters" are mentioned but are described no further (Weidinger 1998, p 327). In the Flims and Tamins rockslides of Switzerland, locally, breccias that originated by cement precipitation after the sturzstrom events are present but to date have not been described by previous authors (own observations). We therefore believe that our case study is the first detailed description of cementation of a rockslide deposit and of its use in minimum-age dating the event. Diagenetic conditions allowing for early cementation probably existed in many rockslide masses, in particular, if the deposit is composed of clasts of carbonate rocks. In such cements, the uranium distribution is easily assessed by β-scanning radiography such that cement suited for age dating can be targeted. In addition, carbonate cements with uranium contents an order of magnitude lower than those described from the Fern Pass rockslide still were readily dateable with the $^{234}U/^{230}Th$ method. Areas with lower regional uranium contents are therefore not basically precluded from this approach to age dating. Comparatively rapid and precise age dating of lithified portions of rockslides and rockfalls by the U–Th method may therefore represent a large and hitherto unexploited source for age determination of catastrophic mass movements.

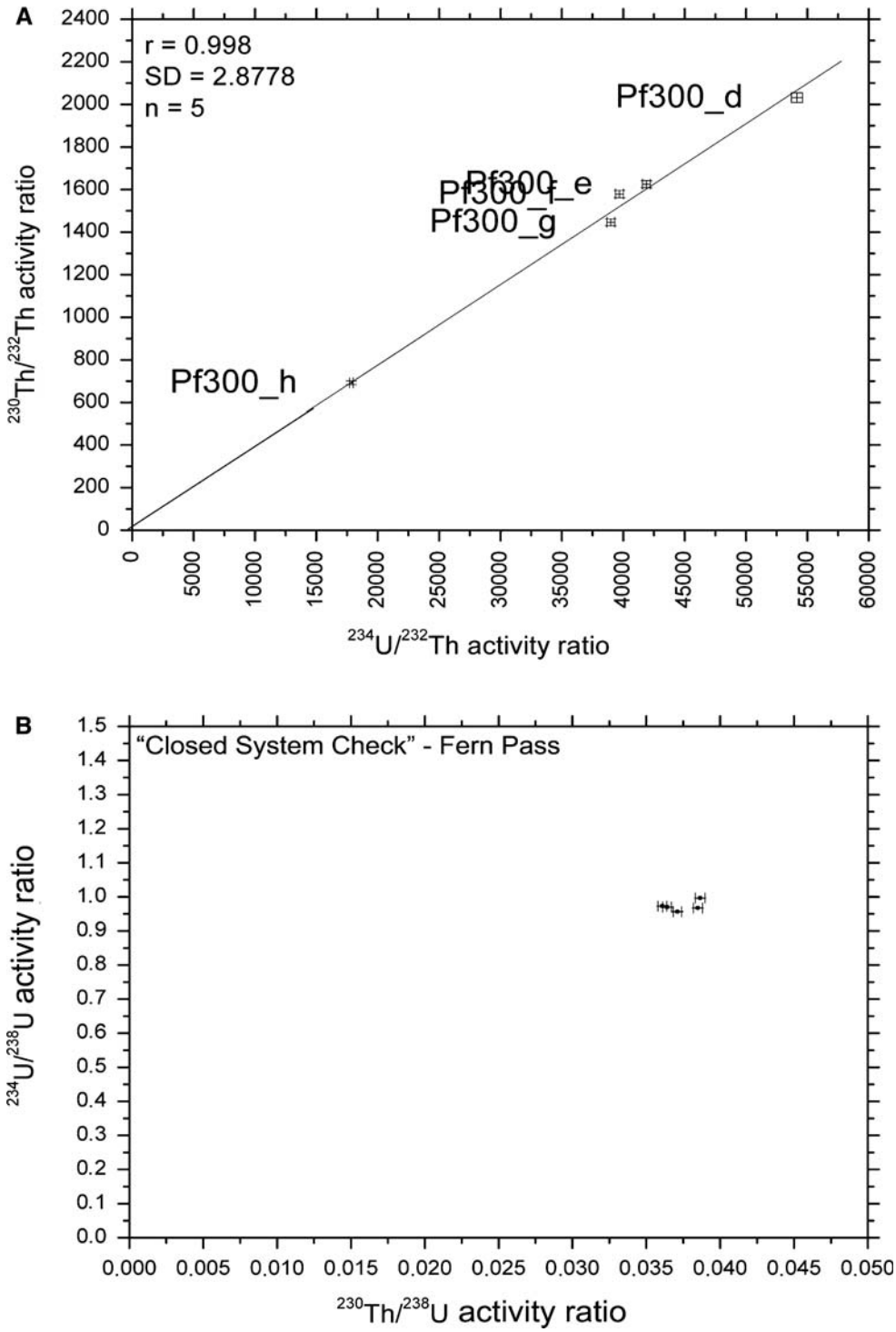

Fig. 7 Thorium–uranium age dating of aragonite cement 1 in a sample from location PF 300 (see Figs. 1, 4a; Table 1). **a** Rosholt diagram with regression line (isochron) of measured activity ratios of subsamples. The error range of the calculated age is two times the standard deviation. **b** Closed system check of subsamples. See Discussion

Conclusions

1. In the southern branch of the Fern Pass rockslide (Northern Calcareous Alps, Austria), carbonate-cemented breccias formed in immediate contact with and along the south-facing flanks of boulders projecting from the rockslide deposit. Boulders with associated breccias are limited to the south-facing side of toma hills.
2. In the breccias, from the vertical to overhanging surface of boulders laterally outwards, both thickness of cements and number of diagenetic phases decrease; beyond about 30 cm laterally off the boulders, the rockslide is unlithified.

Table 4 Contents in uranium and thorium of aragonite cement 1 of sub-samples to sample PF 300 (cf. Table 2)

Sample name	U[a] (ppb)	2σ	Th[b] (ppb)	2σ	(^{234}U/^{238}U)[c]	2σ	(^{238}U/^{232}Th)[c]	2σ	(^{234}U/^{232}Th)[c]	2σ
PF 300_d	170977.8	390.7	9.3	0.1	0.970	0.000	55803.610	470.000	54141.444	456.593
PF 300_e	179444.3	380.2	12.5	0.1	0.957	0.000	43785.275	343.009	41887.209	328.782
PF 300_f	152626.4	405.4	11.3	0.1	0.968	0.001	41018.229	328.318	39689.235	319.079
PF 300_g	110651.9	323.4	8.4	0.1	0.973	0.001	40082.076	328.017	38986.147	320.077
PF 300_h	95223.6	226.2	16.1	0.1	0.996	0.001	17915.773	156.280	17852.460	156.239

Sample name	(^{230}Th/^{232}Th)[c]	2σ	(^{230}Th/^{238}U)[c]	2σ	(^{230}Th/^{234}U)[c]	2σ	(^{230}Th/^{234}U)	2σ
PF 300_d	2031.744208	22.935	0.036	0.000	0.037528114	0.00030744	1.4336E-05	1.20743E-07
PF 300_e	1624.930965	17.222	0.037	0.000	0.038794579	0.000300958	1.8271E-05	1.43133E-07
PF 300_f	1578.819017	16.877	0.038	0.000	0.039781134	0.000320416	1.95035E-05	1.5611E-07
PF 300_g	1446.466647	15.878	0.036	0.000	0.037103566	0.000312731	1.9959E-05	1.63338E-07
PF 300_h	692.3309136	8.177	0.039	0.000	0.038782269	0.000336335	4.46534E-05	3.89513E-07

[a] ppb U = $\sum$ ^{238} U + ^{236} U + ^{234} U

[b] ppb Th = $\sum$ ^{229} Th + ^{230} Th + ^{232} Th

[c] Compared with previously accepted decay constants, activity ratios of 234U/*** are lower by a factor of 0.996925, and activity ratios of 230Th/*** are lower by a factor of 0.99579

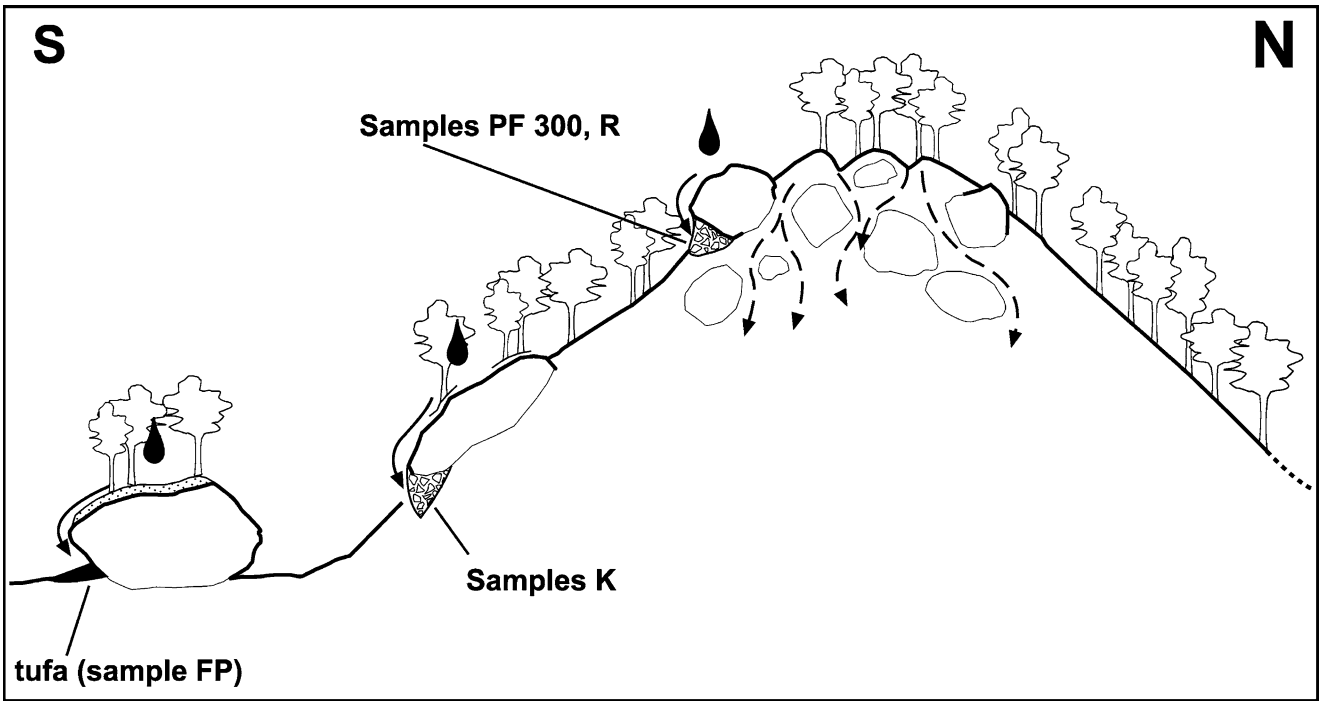

Fig. 8 Schematic summary of diagenetic system of the described breccias and tufas. Along the southern slope of toma hills, boulders situated in the upper but not topmost part of the hills guide surface runoff (rain, melting snow) towards their downhill flanks. There, in local runoff tails in the immediate vicinity downslope of the southern-exposed side of boulders, both supply and retention of water and concentration of pore water by evaporation are balanced thus that precipitation of aragonite and calcite cements can take place. Where meteoric water runoff is not influenced by boulders, pore water readily percolates down to deeper levels within the rockslide deposit (*dashed lines*). In addition, the downslope understorys of boulders located on the northern slope of toma hills are devoid of breccias. Below the south-facing, overhanging surfaces of large boulders that today are covered by soil vegetated by trees, bushes and grass, short ledges of tufa limestone precipitate

3. The original rockslide deposit was rich in carbonate-rock flour produced by dynamic disintegration. Upon atmospheric precipitation, instead of readily percolating down to deeper levels within the rockslide deposit, water shed onto projecting boulders is collected and guided towards the downslope flank of boulders. Where this collected surface runoff entered the unlithified rockslide deposit, dissolution of part of the rock flour resulted in Ca–(Mg)–HCO_3^- waters. The collection

of surface runoff by the boulders results in "haloes" of increased pore-water presence along their downhill flanks. In addition, along the downhill flanks of boulders, water that slowly seeps out of joints within the boulders contributes to keeping the pore space wet. Along the southern side of the toma hills, on the southern (downslope) flank of boulders, the combined effects of prolonged presence of Ca–(Mg)–HCO_3^- pore waters and more intense evaporation in turn resulted in supersaturation for calcium carbonate, allowing for cement precipitation. Early aragonite cement precipitated as a result of dissolved Mg^{2+} and/or high supersaturation for $CaCO_3$. Later, only crystalline calcite cements and/or crusts of micritic cement precipitated. Phases of cement precipitation are separated by phases of dissolution. The cements and their geometrical relationships record fluctuations between essentially phreatic and vadose conditions and between under- and supersaturation for calcium carbonate. Since the rockslide event, the pace of cementation seems to have slowed.

4. $^{234}U/^{230}Th$ age dating of a fringe of early formed uranium-rich aragonite cement indicates a precipitation age of $4{,}150 \pm 100$ years. This age fully overlaps with ^{36}Cl-exposure ages of sliding planes at the scarp and with ^{14}C-dated rockslide-dammed torrent deposits, both determined by other authors. The U–Th age presently is the most precise proxy (minimum age) of the rockslide event age.
5. Localised meteoric lithification of rockslides by aragonite and/or by calcite cements may be common but as yet has not been systematically searched for. U–Th dating of cements represents a source for comparatively rapid, precise and inexpensive determination of minimum ages of catastrophic mass movements.

Acknowledgments Financial support from project 16114-NO6 "Quaternary talus, Northern Calcareous Alps" of the Austrian Research Foundation (to DS) and from project A 2.3 "Process analyses of unstable slopes" of alpS Center for Natural Hazard Management (to CP) is gratefully acknowledged. Ulrich Haas, Bayerisches Landesamt für Umwelt (München) provided us with the first hints on breccias of the Flims rockslide. Axel Munnecke, Erlangen, and Hildegard Westphal, Bremen, are thanked for detailed reviews.

References

Abele G (1964) Die Fernpaßtalung und ihre morphologischen Probleme. Tübing Geogr Stud 12:1–123

Abele G (1974) Bergstürze in den Alpen.Ihre Verbreitung, Morphologie und Folgeerscheinungen. Wissenschaftl Alpenvereinshefte 25:1–230

Abele G (1997) Rockslide movement supported by the mobilization of groundwater-saturated valley floor sediments. Z Geomorph NF 41:1–20

Aharon P (1988) Oxygen, carbon and U-series isotopes of aragonites from Vestfold Hills, Antarctica: clues to geochemical processes in subglacial environments. Geochim Cosmochim Acta 52:2321–2331

Ampferer O (1904) Die Bergstürze am Eingang des Ötztales und am Fernpaß. Verh d Geol R-A 1904:73–87

Ampferer O (1924) Erläuterungen zur Geologischen Spezial-Karte der Republik Österreich, Blatt Lechtal (5045). Geol B-A, Vienna, p 55

Antognigni M, Volpers R (2002) A late Pleistocene age for the Chironico rockslide (Central Alps, Ticono, Switzerland). Bull Appl Geol 7:113–125

Berner RA (1975) The role of magnesium in the crystal growth of calcite and aragonite from sea water. Geochim Cosmochim Acta 39:489–504

Brandner R, Poleschinski W (1986) Stratigraphie und Tektonik am Kalkalpensüdrand zwischen Zirl und Seefeld in Tirol. Jahresber Mitt Oberrheinischen Geol Ver, N F 68:67–92

Chafetz HS, Patrick FR, Utech NM (1991) Microenvironmental controls on mineralogy and habit of $CaCO_3$ precipitates: an example from an active travertine system. Sedimentology 38:107–126

Debaene G (2003) Uranium-series dating of marly sediments: applications to Jaroszów fossil lake (SW Poland). Geochronometria 22:15–26

Delago L (2005) Geologie des Streifens Törl-Hinterhornalm (Nördliche Kalkalpen, Tirol). Unpubl Diploma thesis, Univ of Innsbruck, 148 pp

Donofrio DA, Brandner R, Poleschinski W (2003) Conodonten der Seefeld-Formation: Ein Beitrag zur Bio- und Lithostratigraphie der Hauptdolomit-Plattform (Obertrias, Westliche Nördliche Kalkalpen, Tirol). Geol-Paläont Mitt Innsbruck 26:91–107

Egli M, Fitze P (2001) Quantitative aspects of carbonate leaching of soils with differing ages and climates. Catena 46:35–62

Eisbacher GH, Brandner R (1996) Superposed fold-thrust structures and high-angle faults, Northwestern Calcareous Alps, Austria. Eclog Geol Helv 89:553–572

Elbracht J (2002) Karbonatische Zementation pleistozäner Lockersedimente NW-Deutschlands. Unpubl PhD Thesis, University of Hannover, 214 pp

Erismann TH, Abele G (2001) Dynamics of rockslides and rockfalls. Springer, Heidelberg, p 316

Frank N, Braum M, Hambach U, Mangini A, Wagner G (2000) Warm period growth of travertine during the last interglaciation in Southern Germany. Quaternary Res 54:38–48

Frisia S, Borsato A, Fairchild IJ, McDermott F, Selmo EM (2002) Aragonite–calcite relationships in speleothems (Grotte de Clamouse, France): environment, fabrics, and carbonate geochemistry. J Sediment Res 72:687–699

Fruth I, Scherreiks R (1982) Hauptdolomit (Norian)—Stratigraphy, palaeogeography and diagenesis. Sediment Geol 32:195–231

Geyh MA (2001) Reflections on the $^{230}Th/^{234}U$ dating of dirty material. Geochronometria 20:9–14

Geyh MA (2005) Handbuch der physikalischen und chemischen Altersbestimmung. Wissenschaftliche Buchgesellschaft, Darmstadt, p 211

Gilchrist AR, Summerfield MA, Cockburn HAP (1994) Landscape dissection, isostatic uplift, and the morphologic development of orogens. Geology 22:963–966

Goldbrunner J, Zötl JG (eds) (1993) Die Mineral- und Heilwässer Österreichs. Springer, Vienna, 324 pp

Gosse JC, Phillips FM (2001) Terrestrial in situ cosmogenic nuclides: theory and application. Quaternary Sci Rev 20:1475–1560

Gundersen LCS, Schumann RR, Otton JK, Dubiel RF, Owen DE, Dickinson KA (1992) Geology of radon in the United States. Geol Soc Am Spec Pap 271:1–16

Gutjahr A, Dabringhaus H, Lacmann R (1996a) Studies of the growth and dissolution kinetics of the $CaCO_3$ polymorphs calcite and aragonite. I. Growth and dissolution rates in water. J Crystal Growth 158:296–309

Gutjahr A, Dabringhaus H, Lacmann R (1996b) Studies of the growth and dissolution kinetics of the $CaCO_3$ polymorphs calcite and aragonite. II. The influence of divalent cation additives on the growth and dissolution rates. J Crystal Growth 158:310–315

Heuberger H (1966) Gletschergeschichtliche Untersuchungen in den Zentralalpen zwischen Sellrain und Ötztal. Wissenschaftl Alpenvereinshefte 20:1–126

Ivy-Ochs S, Heuberger H, Kubik PW, Kerschner H, Bonani G, Frank M, Schlüchter C (1998) The age of the Köfels event. Relative, ^{14}C and cosmogenic isotope dating of an early Holocene landslide in the Central Alps (Tyrol, Austria). Z Gletscherkd Glazialgeol 34:57–68

Jerz H, Poschinger Av (1995) Neueste Ergebnisse zum Bergsturz Eibsee-Grainau. Geol Bavarica 99:383–398

Kaufman A (1993) An evaluation of several methods for determining $^{230}Th/^{234}U$ ages in impure carbonates. Geochim Cosmochim Acta 57:2303–2317

Kaufman A, Broecker WS (1965) Comparison of ^{230}Th and ^{14}C ages for carbonate materials from lakes Lahontan and Bonneville. J Geophys Res 70:4039–4054

Köster J, Fries W, Bechstädt T, Kulke H (1989) Kerogenreiche und bituminöse Einschaltungen im Hauptdolomit (Obertrias, Ostalpen): Modell eines karbonatischen Muttergesteins. Abschlußbericht zum DGMK-Projekt 361:305

Krüse K (1926) Beiträge zur Kenntnis der Radioaktivität der Mineralquellen Tirols. VII. Mitteilung. Jb Geol B-A 76:81–96

Krüse K (1937) Beiträge zur Kenntnis der Radioaktivität der Mineralquellen Tirols (VIII. Mitteilung mit einer Gesamtübersicht der bisherigen Untersuchungen). Jb Geol B-A 87:41–56

Krüse K (1940) Beiträge zur Kenntnis der Radioaktivität der Mineralquellen Tirols (IX. Mitteilung und Schluß). Mitt Reichstelle f Bodenforschung (N F Jb Geol B-A) 1:69–80

Laya HA, De La Pena JA, Benayas J (1992) Neoformed aragonite in clay soils on Keuper materials from east-central Spain. J Soil Sci 43:401–407

Lin JC, Broecker WS, Anderson RF, Hemming S, Rubenstone JL, Bonani G (1996) New $^{230}Th/^{234}U$ and ^{14}C ages from Lake Lahontan carbonates, Nevada, USA, and a discussion of the origin of initial thorium. Geochim Cosmochim Acta 60:2817–2832

Ludwig KR, Titterington DM (1994) Calculation of $^{230}Th/^{234}U$ isochrons, ages, and errors. Geochim Cosmochim Acta 58:5031–5042

Mallick R (2000) Entwicklung einer Mikrobeprobung zur Th/U-Datierung und Anwendung an quartären Travertinen aus dem Thüringer Becken. Unpubl PhD Thesis, University of Heidelberg, 167 pp

Mallick R, Frank N (2002) A new technique for precise uranium-series dating of travertine micro-samples. Geochim Cosmochim Acta 66:4261–4272

Meldrum FC, Hyde ST (2001) Morphological influence of magnesium and organic additives on the precipitation of calcite. J Crystal Growth 231:544–558

Ostermann M (2006) Thorium–uranium age-dating of "impure" carbonate cements of selected Quaternary depositional systems of western Austria: results, implications, problems. Unpubl PhD Thesis, University of Innsbruck, 173 pp

Ostermann M, Sanders D, Kramers J (2006) U-Th age dating of carbonate cement in Quaternary talus successions, Northern Calcareous Alps (Austria). In: Pangeo Austria 2006. Innsbruck Univ Press Conf Series, Innsbruck, pp 235–236

Patzelt G, Poscher G (1993) Der Tschirgant-Bergsturz. Arbeitstagung 1993 Geol B-A, Geologie des Oberinntaler Raumes - Schwerpunkt Blatt 144 Landeck. Exkursion D:206–213

Pollet N, Schneider J-LM (2004) Dynamic disintegration processes accompanying transport of the Holocene Flims sturzstrom (Swiss Alps). Earth Planet Sci Lett 221:433–448

Prager C (2005) Relevance of dating deep seated mass movements: evidence from the Holocene Fernpass-rockslide (Northern Calcareous Alps, Tyrol, Austria). Geophys Res Abstr 7:02729, EGU 2005, Vienna

Prager C, Zangerl C (2005) Kinematics of a long run-out rockslide: a case study from the Fernpass-region (Northern Calcareous Alps, Tyrol, Austria). Geophys Res Abstr 7:02737, EGU 2005, Vienna

Prager C, Patzelt G, Ostermann M, Ivy-Ochs S, Duma G, Brandner R, Zangerl C (2006a) The age of the Fernpass rockslide (Tyrol, Austria) and its relation to dated mass movements in the surrounding (abstr.). In: Pangeo Austria 2006. Innsbruck Univ Press Conf Series, Innsbruck, pp 258–259

Prager C, Krainer K, Seidl V, Chwatal W (2006b) Spatial features of Holocene sturzstrom-deposits inferred from subsurface investigations (Fernpass rockslide, Tyrol, Austria). Geo Alp 3:147–166

Probst G, Brandner R, Hacker P, Heiss G, Prager C (2003) Hyrogeologische Grundlagenstudie Westliche Gailtaler Alpen/ Lienzer Dolomiten (Kärnten/Osttirol). Steir Beitr Hydrogeol 54:5–62

Purtscheller F, Pirchl T, Sieder G, Stingl V, Tessadri T, Brunner P, Ennemoser O, Schneider P (1995) Radon emanation from giant landslides of Koefels (Tyrol, Austria) and Lang Tang Himal (Nepal). Environ Geol 26:32–38

Railsback LB, Brook GA, Chen J, Kalin R, Fleisher CJ (1994) Environmental controls on the petrology of a late Holocene speleothem from Botswana with annual layers of aragonite and calcite. J Sediment Res A64:147–155

Rosholt N (1976) $^{230}Th/^{234}U$ dating of travertines and caliche rinds. Geol Soc Am Abstr Progr 8:1079

Sanders D (2001) Spring tufas and cemented slope deposits in gorges of the western Northern Calcareous Alps, Tyrol: an interim overview. Fifth Internat Workshop of Alpine Geological Studies, Obergurgl (Austria). Geol-Paläont Mitt Innsbruck 25:181–182

Sanders D, Unterwurzacher M, Rüf B (2006a) Microbially-induced calcium carbonate in tufas of the western Eastern Alps: a first overview. Geo Alp 3:167–189

Sanders D, Ostermann M, Kramers J, Unterwurzacher M (2006b) Wood, petrified by calcium-carbonate permineralization, in fossil spring tufas of the western Eastern Alps. In: Pangeo Austria 2006. Innsbruck Univ Press Conf Series, Innsbruck, pp 293–294

Sarnthein Rv (1940) Moor- und Seeablagerungen aus den Tiroler Alpen und ihre waldgeschichtliche Bedeutung. II. Teil: Seen der Nordtiroler Kalkalpen. Beih Botan Centralbl LX Abt B(3):437–492

Schmid SM, Fügenschuh B, Kissling E, Schuster R (2004) Tectonic map and overall architecture of the Alpine orogen. Eclogae geol Helv 97:93–117

Sletten RS (1988) The formation of pedogenic carbonates on Svalbard: The influence of cold temperatures and freezing. In: Senneset K (ed) Permafrost. Fifth Int Conf Permafrost Proc 1:467–472

Spötl C, Unterwurzacher M, Mangini A, Longstaffe FJ (2002) Carbonate speleothems in the dry, inneralpine Vinschgau valley, northernmost Italy: witnesses of changes in climate and hydrology since the Last Glacial Maximum. J Sediment Res 72:793–808

Spötl C, Vennemann T (2003) Continuous-flow isotope ratio mass spectrometric analysis of carbonate minerals. Rapid Comm Mass Spectrom 17:1004–1006

Summerfield MA (1991) Global geomorphology. Longman Scientific & Technical, Essex, p 537

Weidinger JT (1998) Case history and hazard analysis of two lake-damming landslides in the Himalayas. J Asian Earth Sci 16:323–331

Weidinger JT, Schramm J-M, Surenian R (1996) On preparatory causal factors, initiating the prehistoric Tsergo Ri landslide (Langthang Himal, Nepal). Tectonophysics 260:95–107

Wilhelmy H (1972) Exogene Morphodynamik. Verwitterung - Abtragung - Tal- und Flächenbildung. Ferdinand Hirt, Coburg, p 223